TOWARDS PREDICTING SLOPE SCALE SNOW TRANSPORT PATTERNS WITH OBJECTIVE COHERENT WIND STRUCTURES

Nikolas Aksamit[1,*], Alexander Prokop[2]

[1] *UiT - The Arctic University of Norway, Tromsø, Norway*
[2] *University of Vienna, Vienna, Austria*

ABSTRACT: Understanding time-varying snow accumulation patterns in complex alpine terrain is crucial for avalanche forecasting. In large countries like Norway with a low density of meteorological measurement stations, area-wide simulations of wind flow and snow accumulation can fill critical gaps in our observational knowledge. At slope scales, snow accumulation patterns are strongly influenced by coherent and recurrent wind flow features that are often driven by atmosphere-mountain interactions. Evidence of the effect of wind structures on snow can be seen around leeside flow separation and recirculation, channelized valley winds, and upslope wind acceleration. These wind features are not stationary, but their repeated presence can play an outsized role in blowing snow redistribution and preferential deposition. While terrain-induced flow features arise from a relatively consistent topography, topography-based erosion and wind loading estimates struggle to capture the complex and non-stationary dynamics of wind-snow coupling. In the present work we utilize high-resolution large eddy simulations of wind flow through a mountain valley in northern Norway to explicitly identify coherent structures in the wind that drive snow deposition and erosion. The strength and location of these wind structures are tested against spatially resolved snow depth maps generated by terrestrial laser scanning having a spatial resolution of 0.5 meters and centimeter accuracy. This provides a validation of specific wind features' cumulative importance in snow surface evolution. We compare these relationships with deposition and erosion estimates that are suggested by common, but subjective, wind diagnostics. This research leverages objective wind structures and a new nonlinear-dynamics-focused approach for predicting snow transport processes in complex terrain for both idealized scenarios and real-time forecasting.

Keywords: blowing snow, preferential deposition, Lagrangian coherent structures, large eddy simulation, laser scanning

1. INTRODUCTION

Wind-driven snow processes cause snow pack heterogeneity that in turn impacts many avalanche practitioners, mountain users, and scientists. Blowing (drifting) snow and preferential deposition can significantly modify mountain snowpacks from hourly to interannual time scales. Increased snow loading from blowing snow and preferential deposition results in temporally and spatially localized avalanche activity, the growth or ablation of snow mountain glaciers, and affects spring melt and flood dynamics.

Common approaches to model blowing snow and preferential deposition rely on relationships with the wind that were originally derived for blowing sand and require stationary winds over horizontally homogeneous and flat terrain (Bagnold, 1941). In snow (re)distribution studies, the friction velocity is typically used as a proxy to represent the force acting on snow particles as it can be correlated with shear stresses in the wind when particular (log-law) velocity profiles occur in stationary winds over flat terrain. In mountainous terrain, these requirements are rarely, if ever, met. In fact, 70% of the Earth's land surface is not considered flat (Strobach, 1991), thus suggesting log-law wind profiles may be the exception and not the rule.

Recent work has characterized the unsteadiness found in mountain winds with specific fluctuations in blowing snow transport and initiation. These fluctuations in the wind are further hypothesized to be connected to coherent gusts and fluid structures, such as those generated by surrounding terrain features in mountainous areas (Aksamit and Pomeroy, 2017, 2018). While Aksamit and Pomeroy (2017) showed statistical connections between the imprint of coherent gusts on turbulent wind measurements and snow transport has been possible, to fully understand the transient and three-dimensional wind structures governing wind-snow coupling, a paradigm shift in the methods used to study blowing snow transport is necessary.

In the present research we investigate new approaches to predicting snow particle accumulation at a mountain study site in northern Norway. We rely on high resolution large eddy simulations and terrestrial laser scanning to relate deposition patterns

*Corresponding author address:
Nikolas Aksamit, Institute for Mathematics and Statistics,
UiT - The Arctic University of Norway
9037 Tromsø, Norway;
tel: +47 77 64 40 01;
email: nikolas.aksamit@uit.no

on multiple aspect with multiple objective and non-objective diagnostics.

2. METHODS

2.1 ROLE OF MATERIAL FRAME INDIFFERENCE

To put the present research in context, we are seeking to understand the influence of transient but coherent flow structures on snow particle accumulation and erosion. These flow structures are *material*. That is, they consist of a volume of air parcels that continuously deform and perfectly follow the wind. Common coherent material structures in geophysical flows include eddies, fronts, and jets. The fluid plume in Figure 1 is another example of such a material flow structure. Coherent structures in the atmosphere are commonly made visible by their influence on tracer particles, such as water vapor patterns in clouds, and ubiquitously exist as the skeleton of fluid flows.

To identify structures in a fluid flow that are responsible for the deformation and organization of that fluid, one must use metrics that are indifferent to Euclidean frame changes (Truesdell and Noll, 2004). These metrics are also referred to as *objective* in the continuum mechanics literature. One can picture this mathematical requirement in the following way: three observers photographing a cloud will identify the exact same cloud geometry even if one observer is stationary on the ground, one is flying in an airplane, and one is circling in a helicopter. In each reference frame (e.g., each photograph), the effect of influential Lagrangian coherent structures on flow tracers (i.e., cloud patterns) does not change, and thus the diagnostics we use to identify the responsible flow structures in our wind data (velocity fields) should not change either. An example of frame indifferent structure identification for a fixed frame and an observer frame undergoing Euclidean frame changes is shown in Figure 1.

Mathematically speaking, we can formulate the requirement of frame-indifference in the following way. Let $\mathbf{x}(t)$ represent a (potentially time-varying) three-dimensional position in the original reference frame, then a generic time-varying Euclidean frame change transforms $\mathbf{x}(t)$ as

$$\mathbf{y}(t) = \mathbf{R}(t)\mathbf{x}(t) + \mathbf{b}(t) \tag{1}$$

where $\mathbf{R}(t)$ is a rotation matrix, and $\mathbf{b}(t)$ represents a translation. Note that $\mathbf{R}(t)$ and $\mathbf{b}(t)$ represent the two kinds of motion possible for observer frame changes on Earth that can be performed without physically distorting the space an observer is measuring.

For a scalar field $P(\mathbf{x}, t)$ to be objective, it must transform under frame changes of the form Eq. 1 as $P(\mathbf{x}, t) = \tilde{P}(\mathbf{y}, t)$. Note that this exactly how temperature and air pressure would change: for a given temperature or pressure field, P, Euclidean frame changes do not alter the values of P, but each measured location may have a different label after the frame change. This can occur, for example, if someone is recording measurements in coordinates based off a city street grid system and later changes to latitude and longitude.

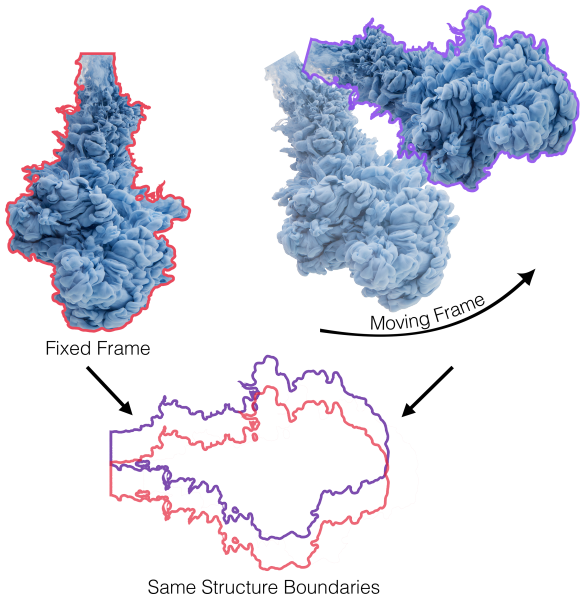

Figure 1: Example of a fluid structure as observed in a fixed frame and a reference frame undergoing translations and rotations. Frame-indifferent structure identification will identify the same material boundaries in both frames.

Previous research has shown that friction velocity and fluctuating-frame-based Reynolds stress metrics are not frame-indifferent scalars (Aksamit et al., 2023). Furthermore, wind vector components and wind speed are also frame-dependent. Therefore, the shapes present in wind speed or friction velocity fields cannot be used to identify the true boundaries of wind flow structures (e.g. gusts) that are responsible for blowing snow transport and preferential deposition organization. The reader is referred to Haller (2023) for further discussion on frame-indifferent diagnostics.

The eigenvectors of the Cauchy-Green strain tensor are frame-indifferent vectors, and the associated eigenvalues are frame-indifferent scalars. The largest Cauchy-Green eigenvalue and eigenvector correspond with the rate and direction of strongest fluid stretching during a period of time. In incompressible fluids, such as boundary layer winds, the direction of the eigenvector is also perpendicular to planes of attraction. The largest Cauchy-Green strain tensor eigenvalue is shown as λ in Figure 2 and is the exponential of the finite-time Lyapnuov exponent (FTLE) (Haller, 2023). Because of the mathematically rigorous and physical meaning of FTLE, we will test FTLE as a means to describe wind and snow accumulation patterns and avoid

the user-ambiguity and correlations necessary with other snow accumulation diagnostics.

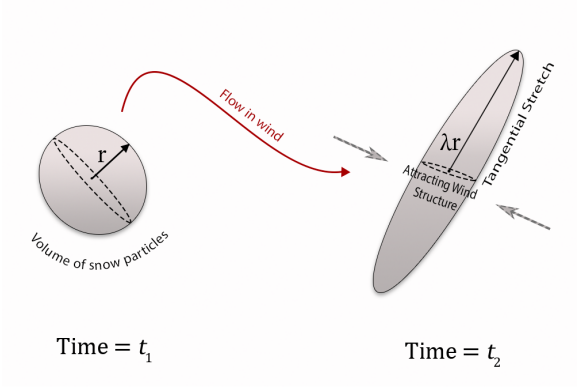

Figure 2: A theoretical spherical collection of snow particles deforms in a wind flow over time with an initial radius vector r stretching to length λr. This sort of deformation and the associated organization of nearby snow particles can be rigorously studied using tools from dynamical systems and continuum mechanics.

2.2 STUDY SITE

Ullstinden is a 1078 m peak at the northern end of a peninsula approximately 45 minutes to the northwest of Tromsø, Norway by car (Figure 3). This location provides a unique geographic opportunity for observations of snowpack evolution as it sits at the confluence of three Arctic valleys in northern Norway and provides line-of-site observations of multiple mountain aspects from a single location. Furthermore, Ullstinden is surrounded on the NW to N to SE by water and open fjords, thus limiting upwind terrain influence for several wind directions. Immediately south of Ullstinden is route Fv864, a paved road that provides year-round access from Tromsø to Oldervik, a village under consistent threat of avalanches from the SE flanks of Ullstinden.



Figure 3: Ullstinden TLS scanning site near Tromsø, Norway with Svarthammartinden and Ullstinden in the middle and left background, respectively. The background terrain corresponds with the yellow scan from Figure 3.

From the roadside parking lot, TLS snow depth measurements are easily obtained up to 4 km away (Figure 4). TLS snow depth maps were achieved following the methodology described by Prokop (2008, 2009). Typical scanning zones can be found in Figure 4 overlaid on the local topography. Each color represents a different mountain with different aspects and varying slope steepness. In this region, winds are predominantly southwesterly in the winter. Figure 5 shows the wind rose of 10 meter wind speeds from ERA 5 reanalysis during the 2023-2024 winter. Currently there are no meteorological stations in the region, though an avalanche focused station was previously operational on a subpeak of Ullstinden.

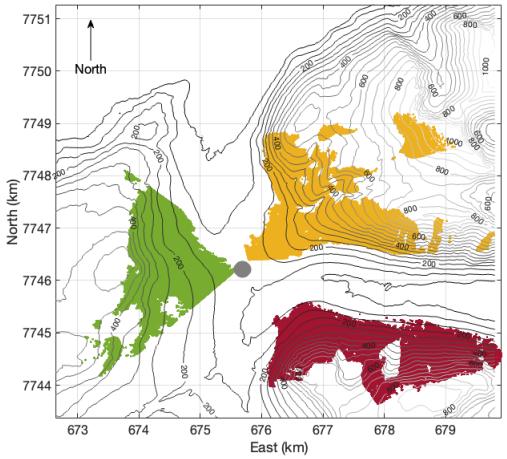

Figure 4: Three zones of TLS scanning site overlaid on topographic map of the Snarbydalen region. Scan origin marked by a grey dot.

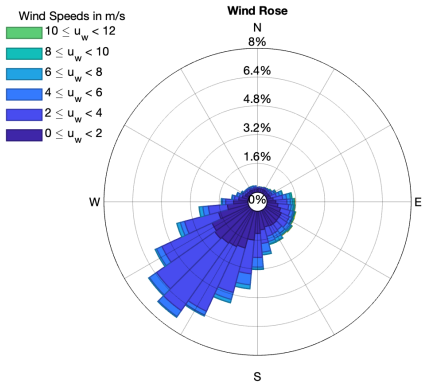

Figure 5: Wind rose of 10 meter wind data from ERA 5 grid cells surrounding the Ullstinden study area during the 2023-2024 winter.

2.3 MODELING FRAMEWORK

We simulated wind in our mountain environment using the PALM large eddy simulation framework

(Maronga et al., 2020). We ran nested PALM simulations around the Ullstinden study site with our largest "root" domain being 73 km × 57 km × 5 km (x, y, z) with an x-y grid resolution of 120 m, and our smallest high-resolution domains that overlap with our TLS zones measuring approximately 2.5 km × 2.5 km with an x-y grid resolution of 5 m and vertical grid spacing of 2 m. (Figure 6). Simulations were run with the turbulence recycling method to reduce computational cost and prevent artifacts from cyclic boundary conditions (Maronga et al., 2020). After 5 hours of simulated flow, the 3D velocity field was output at 1 second intervals.

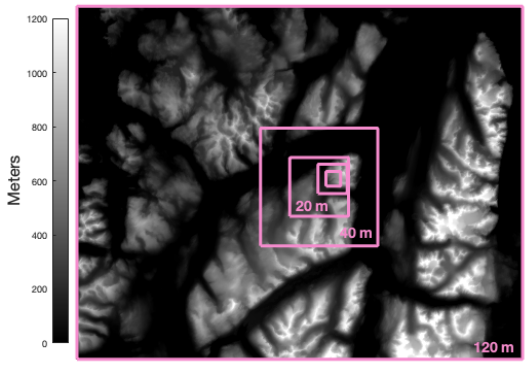

Figure 6: Topography of nested wind simulations for one of the three scanning locations. Domain boundaries are drawn in pink with domain resolution noted in the bottom corner. The two innermost domains at 10 meter and 5 meter resolution are not labeled for clarity. Innermost domain corresponds with yellow scan from Figure 3.

To understand the role of near surface Lagrangian coherent structures on the distribution of snow particles, we release a uniform grid of snow particles initially 20 meters above the snow surface. We approximate the equations of motion of the finite size and finite density snow particles in this turbulent flow via the Maxey-Riley equations (Maxey and Riley, 1983). We simplify the full MR equations by assuming the ratio of snow particle radii to atmospheric eddy sizes is small. A simplified version of the MR equation of motion for a snow particle at position $\mathbf{x}(t)$ with velocity $\mathbf{v}$ in a wind field $\mathbf{u}$ can be written as

$$\dot{\mathbf{x}}(t) = \mathbf{v}(\mathbf{x}, t) \tag{2}$$

$$\dot{\mathbf{v}} = -\mu(\mathbf{v} - \mathbf{u}) + \frac{3R}{2}\frac{D\mathbf{u}}{Dt} + \left(1 - \frac{3R}{2}\right)\mathbf{g} \tag{3}$$

where $R = 2\rho_f/(\rho_f + 2\rho_p)$, $St = (2/9)(a/L)^2\mathrm{Re}$, $\mu = R/St$, ρ_f and ρ_p are the fluid and particle densities, respectively, and Re is the particle Reynolds number. Note that we rely on an assumption that $Re < 1$ in order to utilize Stokes' drag, which will be reassessed in future research.

3. RESULTS

After performing a bare ground LiDAR scan in October 2023, we collected one round of snow depth measurements in April 2024 to identify regions with significant seasonal accumulation. We then simulated wind flow for the average wind direction over the winter (see, e.g., Figure 5). This provided a rough approximation of terrain-generated wind features that were present during the winter. We utilized neutral atmospheric conditions with no terrain roughness elements (e.g., vegetation). Additionally, we enforced a low (2 m/s) geostrophic wind speed to prevent any need for blowing snow modeling.

Uniform grids of snow particles were seeded 20 meters above the snow surface and were allowed to fall for 20 seconds or until they hit the ground. After twenty seconds, the final position of snow particles was analyzed to identify regions of increased and decreased accumulation (preferential deposition). This process was repeated 10 times over different time windows and the cumulative results were assessed. Figure 6 (top) shows the relative change in particle density immediately above the snow surface for the yellow scan area from Figure 4. Some preferential deposition is evident with this rough analysis of accumulation, but the low signal-to-noise ratio prevents clear interpretation of snowfall patterns. These density changes can be compared with Figure 7 (bottom) which details the April 2024 TLS snow depth for a subset of the simulation domain. The red line in Figure 7 outlines the boundary of the scanning site for easier comparisons.

In contrast, we calculate the FTLE field from the snow particle trajectories and find much clearer patterning on the ridgetop and leeward sides of multiple ridges and drainages on Ullstinden (Figure 7, middle). Large FTLE values suggest regions of large stretching and shear in the snow particle fields, whereas low FTLE values represent potential compression, enhanced accumulation, or quiescent flow conditions. Much of the seasonal leeside accumulation in the TLS data is present in the FTLE field, even though FTLE was calculated for only one wind direction over 100 seconds of simulation.

Two major differences between the TLS snow depth field and FTLE can be found. First, around the 400 meter elevation band we have enhanced accumulation in the TLS data, with only some leeward regions exhibiting the same relatively low FTLE values. This can be attributed to the lack of vegetation in our PALM simulations at this elevation band which can be clearly seen in the background of Figure 3. Future studies will include increased roughness due to vegetation and will likely mitigate these differences. The second major difference occurs near the summit of Ullstinden where there is increased TLS snow depth, but relatively high FTLE. This may be attributed to the orographic effects on precipitation

rates spanning a 1000 meter peak, from accumulation patterns caused by the other two Cauchy-Green eigenvalues, or deposition during storms with a different wind flow .

We compare the efficacy of our inertial particle analysis with two standard meteorological metrics used for snow deposition studies, the surface friction velocity and 2 meter wind speed. In Figure 8 we plot the same snow depth data and use two colormaps for the friction velocity and wind speed. We transition from a grayscale colormap to the previous purple colormap at approximate transport thresholds. There is some correlation between the patterns of friction velocity, wind speed, and snow depth, but the vast majority of friction velocity and wind speed values are well below any sort of transport thresholds.

4. CONCLUSIONS

The present research suggests a modern rethinking of snow accumulation and erosion diagnostics may be beneficial for those interested in generating spatially and temporally resolved snow depth fields. While some seasonal accumulation patterns were approximated using only 2 minutes of simulated wind flow, future research should focus on event specific dynamics to better understand the physical processes under investigation. Current improvements underway include tailoring the Maxey-Riley equations for snow transport, incorporating surface vegetation in PALM simulations, and comparing with existing high resolution wind products.

Improved downscaling of snow depth heterogeneity would have significant impact on hydrological, glaciological, and climatological studies. For snow and avalanche research, site specific improvements in accumulation modeling, such as detailed here, may result in more immediate positive benefits for forecasting as well as hazard mapping.

References

Aksamit, N. O. and Pomeroy, J. W.: The Effect of Coherent Structures in the Atmospheric Surface Layer on Blowing-Snow Transport, Boundary-Layer Meteorology, 167, 1–23, doi:10.1007/s10546-017-0318-2, 2017.

Aksamit, N. O. and Pomeroy, J. W.: Scale Interactions in Turbulence for Mountain Blowing Snow, Journal of Hydrometeorology, 19, 305–320, doi:10.1175/JHM-D-17-0179.1, URL http://journals.ametsoc.org/doi/10.1175/JHM-D-17-0179.1, 2018.

Aksamit, N. O., Katurji, M., and Zhang, J.: Approaching coherent turbulence and the roll-cell transition with Lagrangian coherent structures and objective fluxes, In Review: Journal of Geophysical Research: Atmospheres, doi:10.21203/rs.3.rs-3407303/v1, 2023.

Bagnold, R.: The Physics of Blown Sand and Desert Dunes, Methuen and Co. Limited, London, 1 edn., 1941.

Haller, G.: Transport Barriers and Coherent Structures in Flow Data: Advective, Diffusive, Stochastic and Active Methods, Cambridge University Press, Cambridge, UK, doi:doi:10.1017/9781009225199, 2023.

Maronga, B., Banzhaf, S., Burmeister, C., Esch, T., Forkel, R., Fröhlich, D., Fuka, V., Gehrke, K. F., Geletič, J., Giersch, S., Gronemeier, T., Groß, G., Heldens, W., Hellsten, A., Hoffmann, F., Inagaki, A., Kadasch, E., Kanani-Sühring, F., Ketelsen, K., Ali Khan, B., Knigge, C., Knoop, H., Krč, P., Kurppa, M., Maamari, H., Matzarakis, A., Mauder, M., Pallasch, M., Pavlik, D., Pfafferott, J., Resler, J., Rissmann, S., Russo, E., Salim, M., Schrempf, M., Schwenkel, J., Seckmeyer, G., Schubert, S., Sühring, M., Von Tils, R., Vollmer, L., Ward, S., Witha, B., Wurps, H., Zeidler, J., and Raasch, S.: Overview of the PALM model system 6.0, Geoscientific Model Development, 13, 1335–1372, doi:10.5194/gmd-13-1335-2020, 2020.

Maxey, M. and Riley, J.: Equations of motion for a small rigid sphere in a nonuniform flow, Physics of Fluids, 26, 883–889, 1983.

Prokop, A.: Assessing the applicability of terrestrial laser scanning for spatial snow depth measurements, Cold Regions Science and Technology, 54, 155–163, doi:10.1016/j.coldregions.2008.07.002, URL http://dx.doi.org/10.1016/j.coldregions.2008.07.002, 2008.

Prokop, A.: Terrestrial laser scanning for snow depth observations: An update on technical developments and applications, ISSW 09 - International Snow Science Workshop, Proceedings, pp. 192–196, 2009.

Strobach, K.: Unser Planet Erde-Usprung und Dynamik, Gebruder Bornträger, 1991.

Truesdell, C. and Noll, W.: The Non-Linear Field Theories of Mechanics, The Non-Linear Field Theories of Mechanics, pp. 1–579, doi:10.1007/978-3-662-10388-3_1, URL http://www.springerlink.com/index/10.1007/978-3-662-10388-3_1, 2004.

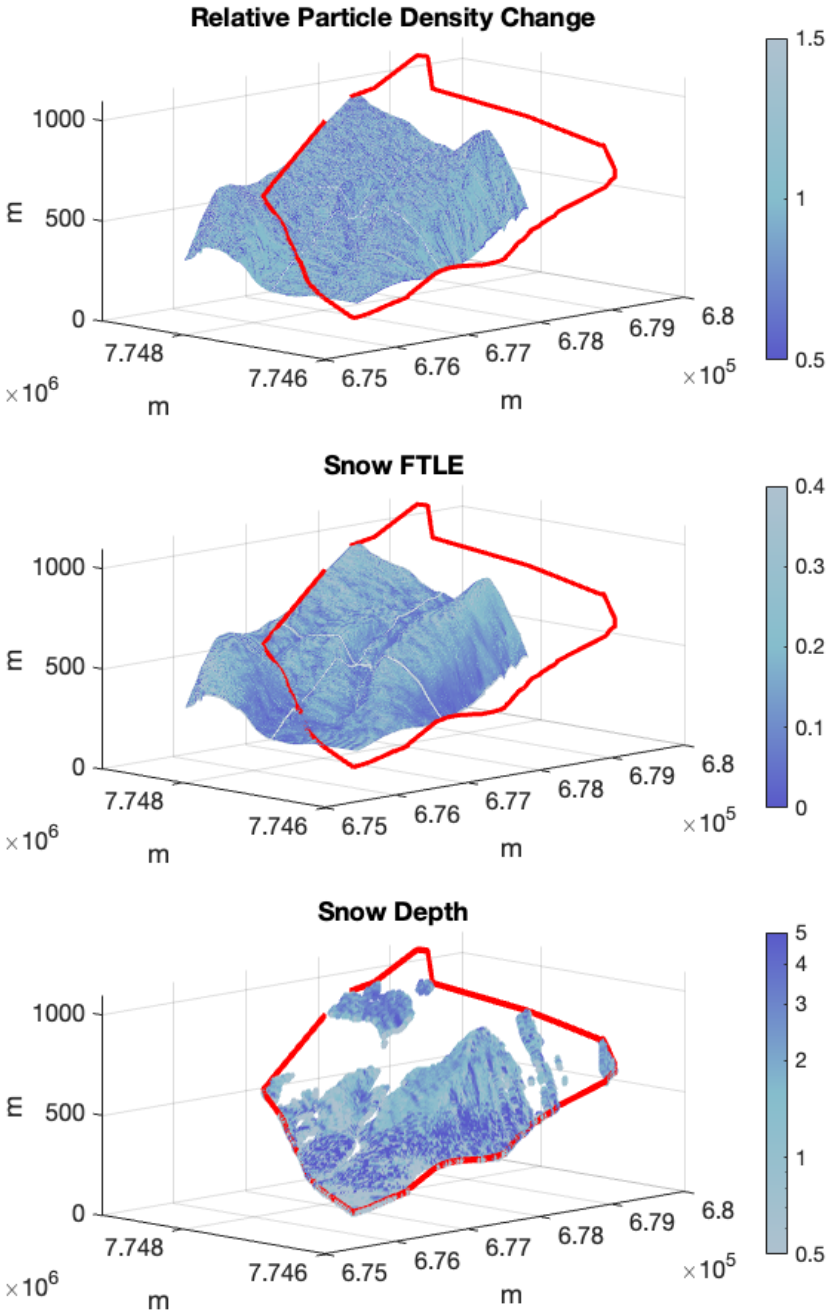

Figure 7: Comparison of average particle density change and finite time Lyapnuov exponents from 10 20-second simulations of snowfall in the lowest 20 meters of the atmosphere. Patterns mimicking springtime snow depth as measured by TLS can be seen in the FTLE fields, whereas relative particle density change poorly resolves the processes. TLS scan boundaries are drawn in red. This domain corresponds with the yellow scan from Figure 3.

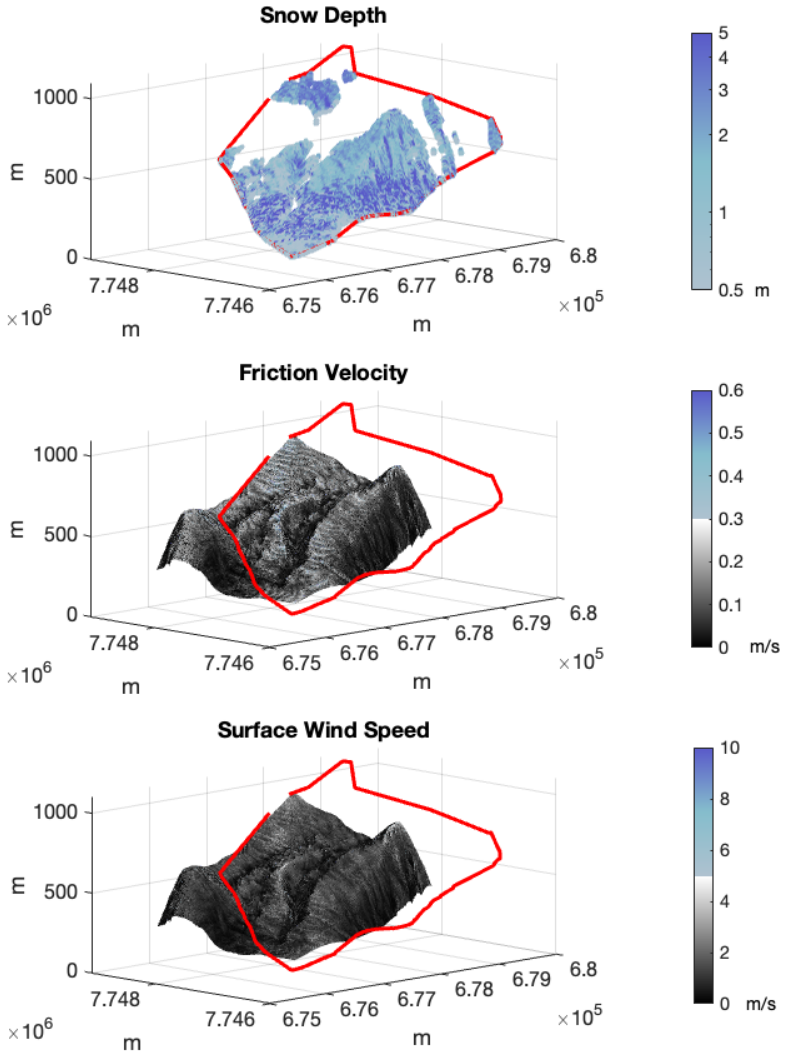

Figure 8: Comparison of average surface friction velocity and 2 meter wind speed with springtime snow depth. Wind diagnostics are calculated using the same 100 seconds of simulation output as from the Lagrangian diagnostics in Figure 7. Both friction velocity and surface windspeed are expected to be below redistribution thresholds (in gray scale), thus limiting our ability to predict deposition patterns.